UC Berkeley
UC Berkeley Previously Published Works

Title

Intercalibration and age of the Alder Creek sanidine 40Ar/39Ar standard

Permalink

Authors

Niespolo, Elizabeth M
Rutte, Daniel
Deino, Alan L
et al.

Publication Date

2017-04-01

DOI

Peer reviewed

Research paper

Intercalibration and age of the Alder Creek sanidine ^{40}Ar/^{39}Ar standard

Elizabeth M. Niespolo [a,b,*], Daniel Rutte [a,b], Alan L. Deino [b], Paul R. Renne [a,b]

[a] Department of Earth and Planetary Science, University of California, Berkeley, CA 94720, USA
[b] Berkeley Geochronology Center, 2455 Ridge Road, Berkeley, CA 94709, USA

ABSTRACT

The accuracy of ^{40}Ar/^{39}Ar geochronology relies in large part on precise and accurate calibration of the ages and K-Ar isotopic compositions of standards. A widely used standard for Quaternary samples, the ~1.2 Ma Alder Creek sanidine (ACs), has published ages spanning a range of ~2%. New measurements of ACs co-irradiated with the Fish Canyon sanidine (FCs) standard and sanidines from astronomically dated Miocene tuffs in Crete and Morocco yield results that enable both (i) a direct calibration of ACs relative to FCs, and (ii) stepwise calibrations between these two standards employing the Miocene intermediaries. Results are summarized by the parameter R_{FCs}^{ACs}, defined as the ratio of (^{40}Ar*/^{39}Ar$_K$) of ACs to FCs, which embodies the fundamental age relationship between these standards that is independent of systematic variables such as decay constants or absolute ages of standards. Our new measurements, executed using three mass spectrometers and various irradiation and analytical protocols, yield a weighted mean $R_{FCs}^{ACs} = 0.041702 \pm 0.000014$ (σ). This result can be combined with previously published determinations of R values for ACs relative to the Miocene tuffs and to FCs to yield a recommended interlaboratory value of $R_{FCs}^{ACs} = 0.041707 \pm 0.000011$. The weighted-mean age of ACs using this interlaboratory value, based on astronomically-calibrated ages of FCs and the Miocene intermediary sanidines, is $t_{ACs} = 1.1848 \pm 0.0006$ Ma ($\pm 0.05\%$). Applying this result to the most precise published ^{40}Ar/^{39}Ar data for the Matuyama-Brunhes geomagnetic polarity reversal yields $t_{MBB} = 780.1 \pm 0.8$ ka. In addition, these new data for ACs support previous conclusions that U-Pb zircon ages from the Alder Creek rhyolite incorporate ~13 ka of pre-eruptive residence time.

© 2016 Elsevier B.V. All rights reserved.

1. Introduction

The ^{40}Ar/^{39}Ar technique is one of the most powerful dating methods available given its potential for high-precision ages and its broad applicability in a multitude of geological settings. However, the accuracy of the technique is limited by our knowledge of the true age and K-Ar isotopic composition of standards (neutron fluence monitors) used to determine the ^{40}Ar*/^{40}K ratios of unknowns through neutron activation analysis. Accuracy concerns are especially critical in the late Neogene, where ^{40}Ar/^{39}Ar ages are evaluated against comparably precise constraints from independent dating methods such as orbital tuning, ^{14}C, or U-series.

Good analytical practice in ^{40}Ar/^{39}Ar dating dictates that the

ages of standards should be as close as possible to the ages of samples being dated in order to minimize mass spectrometric biases potentially imposed by divergent ion beam intensities and their ratios. Accordingly, Turrin et al. (1994) proposed sanidine from the early Pleistocene Alder Creek rhyolite in the Napa-Sonoma volcanic province of northern California as a Quaternary (sensu lato) ^{40}Ar/^{39}Ar standard. This sanidine (ACs) was proposed in part because the lava was emplaced during the Cobb Mountain geomagnetic polarity event, which can in principle be dated independently by orbital tuning methods. Turrin et al. (1994) obtained an age of 1.186 ±0.006[1] Ma for this sanidine, based on an age of 27.84 Ma for the neutron fluence monitor used, sanidine from the Fish Canyon Tuff of Colorado (FCs). Renne et al. (1998) reported an age of 1.194 ± 0.007 Ma using 28.02 Ma for FCs, identical to the value reported by Turrin et al. (1994) when recalculated to the same

* Corresponding author. Department of Earth and Planetary Science, University of California, Berkeley, CA 94720, USA.
E-mail address: eniespolo@berkeley.edu (E.M. Niespolo).

[1] All uncertainties in this paper are stated at the level of σ.

Table 1
Summary of R_{FCs}^{ACs} from published data reflect excess scatter yielding an imprecise and potentially inaccurate calibration of ACs.

Publication	R	±(abs.)	±(%)
Turrin et al. (1994)	0.04229	0.00021	0.50%
Renne et al. (1998)	0.04229	0.00006	0.14%
Nomade et al. (2005)	0.04230	0.00006	0.14%
Coble et al. (2011)	0.04180	0.00021	0.50%
McDougall et al. (2012)	0.04189	0.0006	1.43%
Rivera et al. (2013)	0.04175	0.00003	0.07%
Phillips & Matchan (2013)	0.04169	0.00002	0.04%
Singer (2014)	0.04185	0.00011	0.27%
Jicha et al. (2016)	0.04176	0.00004	0.09%

age for FCs. A subsequent study (Nomade et al., 2005) of sanidine from a recollected sample yielded an age of 1.193 ± 0.001 Ma also using 28.02 Ma as the age of FCs, indistinguishable from the prior two results.

More recently, several ages for ACs relative to FCs have been published by Coble et al. (2011), McDougall et al. (2012), Phillips and Matchan (2013), Rivera et al. (2013), and Jicha et al. (2016) that are distinct from the previous results as summarized by Nomade et al. (2005). Part of this inconsistency is due to different ages ascribed to the FCs standard upon which these ages are based; this is mainly because $^{40}Ar^*$ concentrations in K-Ar dated primary standards ('first-principals' standards calibrated through separate K and Ar measurements) weren't well known enough to resolve interlaboratory differences between calibrations of FCs. To isolate the effects of different calibrations versus analytical variability, we focus herein on Ar isotope systematics rather than computed ages. A simple metric for the age relationship between any two samples, which is independent of irradiation time or age assumed for the anchoring standard (in this case, FCs), is the R-value introduced by Renne et al. (1998):

$$R_{FCs}^{ACs} = \frac{\left(e^{\lambda t_{ACs}} - 1\right)}{\left(e^{\lambda t_{FCs}} - 1\right)} = \frac{(^{40}Ar^*/^{39}Ar_K)_{ACs}}{(^{40}Ar^*/^{39}Ar_K)_{FCs}} \quad (1)$$

where λ is the total ^{40}K decay constant, $^{40}Ar^*$ is the proportion of ^{40}Ar that is radiogenic, and $^{39}Ar_K$ is the proportion of ^{39}Ar that is produced from ^{39}K during neutron activation. R, which relates the age of ACs to that of FCs, may be determined either from corrected mass spectrometric data or from reported ages. For convenience, we define a parameter F as:

$$F \equiv {}^{40}Ar^*/^{39}Ar_K \quad (2)$$

such that

$$R_{FCs}^{ACs} = \frac{F_{ACs}}{F_{FCs}} \quad (3)$$

Table 1 shows a summary of R for the published ACs to FCs data. The population of R exhibits excess scatter about the weighted mean (0.041787 ± 0.000014), as indicated by a mean square of weighted deviates (MSWD, equivalent to the reduced chi-squared statistic) of 39.9. This indicates that the observed scatter is more than expected by the stated analytical uncertainties of the data (the data are 'overdispersed').

A contributing factor to the overdispersion may be the underestimation of error introduced in attempting to measure co-irradiated samples of ACs and FCs with $^{40}Ar/^{39}Ar$ ratios differing by a factor of ~24, which requires inevitable compromises in irradiation times and attendant differences in the behavior of ion beams, particularly of ^{40}Ar and ^{39}Ar. In order to mitigate these

difficulties, part of this study is designed to calibrate the ACs standard with a sample intermediate in age between ACs and FCs, allowing the R_{FCs}^{ACs} value to be determined stepwise using the relationship

$$R_{FCs}^{ACs} = R_X^{ACs} \cdot R_{FCs}^{X} \quad (4)$$

For this purpose, sample "X" can be completely arbitrary provided it is intermediate in age between ACs and FCs and yields reproducible Ar isotope data. Ideally, it should be similar in chemical composition to ACs and FCs to minimize differences in irradiation-induced interference corrections; i.e., a sanidine is most suitable.

For this study, ACs and FCs were co-irradiated and analyzed with sanidines from an ignimbrite of the Messâdit section, Melilla basin, Morocco (Mes4) and sanidine from the A1 distal fallout tephra of the Faneromeni section at Sitia, Crete, Greece (A1). These tuffs have independent orbitally tuned ages of 6.791 ± 0.005 Ma and 6.943 ± 0.0025 Ma, respectively (Kuiper et al., 2008; Rivera et al., 2011). The Messâdit sanidine was previously analyzed by Kuiper et al. (2008) and serves in large part as basis for an orbitally tuned age of 28.201 ± 0.023 Ma for FCs. The A1 sanidine was used by Kuiper et al. (2004) and Rivera et al. (2011) to determine ages of 28.21 ± 0.04 and 28.172 ± 0.014 Ma, respectively, for FCs. Thus, in addition to serving as intermediaries in the stepwise intercalibration of ACs and FCs, independent orbitally tuned ages can be determined for ACs through Mes4 and A1. The calibration of ACs using astronomically tuned standards instead of primary standards minimizes the introduction of uncertainty from decay constants into the final age calculation for young Cenozoic samples (Kuiper et al., 2008). By varying grain size, irradiation time and degassing schedule (i.e., step-heating versus total fusion), and employing multi- as well as single-collector mass spectrometry, we test for the possible effects of recoil, varying ion-beam behavior, and detector intercalibration.

In addition to the stepwise intercalibration of ACs with FCs through the two intermediaries (Mes4 and A1), new direct ACs/FCs intercalibration data are presented for comparison. As shown below, these various approaches yield consistent results.

2. Methods

2.1. Samples

2.1.1. ACs (ACs-2)

The Alder Creek sanidine (ACs) was obtained from the same sample (ACs-2) of the Alder Creek rhyolite analyzed by Nomade et al. (2005) from Cobb Mountain, California (N38°48′6.1″, W122°45′05.4″). Phenocrystic sanidine prepared from this sample has been widely distributed to $^{40}Ar/^{39}Ar$ geochronology community worldwide. The Alder Creek rhyolite was erupted during the Cobb Mountain geomagnetic polarity subchron, whose age has been estimated by orbital tuning of marine sediments between 1.173 and 1.185 Ma (Horng et al., 2002) and 1.190 to 1.215 Ma (Channell et al., 2002; Shackleton et al., 1990).

2.1.2. Mes4 (ME00-2)

Phenocrystic sanidine from sample ME00-2 (N35°21′5.48″, W3°1′26.93″) is from an ignimbrite in the Messâdit section of Kuiper et al. (2008), and it is equivalent to sample Mes4 of that study. The tuff occurs near the base of the sequence and is ~5m thick, distinctly thicker than any other tuff in the section. The sample, analyzed on a MAP 215-C instrument (MAP 1) and a MAP215-50 instrument dubbed "Nexus," was collected by P.R.R. accompanied by K. Kuiper in 2000. A second sample (analyzed on

Table 2
Size fractions and irradiation times for each disk. See Fig. 1 for disk configurations and sample arrangements.

Irradiation			Size fractions (μm)			
Number	Time (h)	Layout	ACs	Mes4	A1	FCs
450PRA	4 h	mixed pits	841–1410	595–841, 841–1410	–	–
424	10 h	separate pits	600–700	500–600	500–600	300–350
452A	3 h	mixed pits	700–840	500–600	–	400–500
449	3 h	mixed pits	700–840	–	–	350–400

the Noblesse) was collected in 2001 by A.L.D., accompanied by K. Kuiper.

2.1.3. A1 (FAN-1)

Sample FAN-1 (N35°13′19.57", E26° 3′59.00") is phenocrystic sanidine from the dacitic-rhyolitic A1 tephra as identified in the Faneromeni marine sapropel cyclostratigraphic section on Crete (FAN-1; Kuiper et al., 2004; Rivera et al., 2011, 2013), collected by A.L.D. accompanied by K. Kuiper in 1999.

2.1.4. FCs

The sample of Fish Canyon Tuff was collected in 1998 (N 37°36.646′, W 106°42.331′) by A.L.D. and C. Swisher. 264 kg of rock were collected and sent to M. Villeneuve at the Geological Survey of Canada for sanidine separation.

2.2. Sample preparation

All samples were crushed, sieved, and washed in distilled water in an ultrasonic bath. Sanidine was separated using a Frantz Isodynamic magnetic separator and heavy liquids. The sanidine concentrates were cleaned with dilute hydrofluoric acid in an ultrasonic bath for 5 min to remove adhering groundmass and handpicked to purity. Size fractions used in the various experiments are listed in Table 2.

2.3. Irradiation

Samples were irradiated in the Cd-lined, in-core CLICIT facility of the Oregon State University TRIGA reactor. Irradiation times are given in Table 2. Fig. 1 shows the layout of the samples in the high-purity Al discs used as sample containers. In three irradiations (450PRA, 452A, and 449) the samples were mixed within individual pits and in one irradiation (424) the samples were irradiated in separate pits. Irradiation 424 contained ACs, FCs, Mes4, and A1 all in separate pits equidistant from the disc center. Planar regressions were fit to the FCs data to determine comparable F values of FCs in pits containing ACs, Mes4, or A1. In irradiation 450PRA, the horizontal (within disc) fluence variations were monitored with additional ACs samples allowing assessment of maximal gradients over
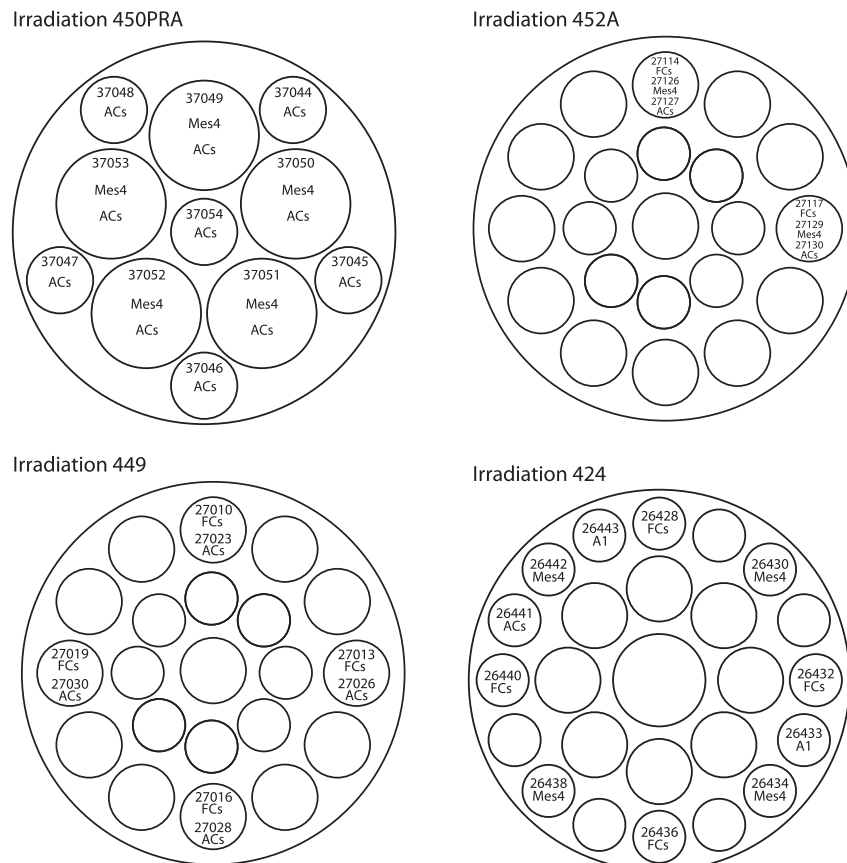
Fig. 1. Disc maps for each of the 18.54-mm aluminum discs showing samples analyzed in this study. ACs and Mes4 samples in irradiation 450PRA have the same lab ID numbers and were distinguished during analysis by ($^{40}Ar*/^{39}Ar_K$).

mixed pits and to evaluate fluence variation between separate pits.

The approximate radiogenic ^{40}Ar concentration ratio of ~6 between ACs and Mes4/A1 and of ~4 between Mes4/A1 and FCs allowed a reasonable compromise in irradiation time, contrasting with an approximate ^{40}Ar concentration difference of ~24 between ACs and FCs. This highlights the advantage of the intermediate intercalibration step using R values in avoiding under- or over-irradiation of one of the samples. We chose irradiation times of 3–4 h—optimized for ACs, Mes4 and A1—for irradiations 450PRA, 452A and 449 and a more FCs-optimized irradiation time of 10 h for irradiation 424. In addition, in irradiation 450PRA the grain sizes of Mes4 and ACs were paired in pits with the intent to yield similarly sized ion beams of ^{40}Ar or ^{39}Ar depending on the size fraction of ACs loaded with Mes4. For equivalently sized samples, ^{39}Ar ion beams after irradiation are similar, while the combination of ACs with a smaller Mes4 fraction yields similarly sized ^{40}Ar ion beams.

Interference corrections were based on the following nucleogenic production ratios (Renne et al., 2015): $(^{40}Ar/^{39}Ar)_K = (7.30 \pm 0.92) \times 10^{-4}$; $(^{37}Ar/^{39}Ar)_K = (2.24 \pm 0.16) \times 10^{-4}$; $(^{38}Ar/^{39}Ar)_K = (1.196 \pm 0.013) \times 10^{-2}$; $(^{39}Ar/^{37}Ar)_{Ca} = (7.02 \pm 0.12) \times 10^{-4}$; $(^{36}Ar/^{37}Ar)_{Ca} = (2.702 \pm 0.004) \times 10^{-2}$; $^{36}Cl/^{38}Cl = (2.628 \pm 0.002) \times 10^2$.

To evaluate fluence gradients over the Al discs, the two distinct irradiation geometries used require separate treatment (Fig. 1). In irradiations 449, 450PRA, and 452A, the various samples were irradiated in mixed pits with depths of 2–3.3 mm and diameters of 3.2–5.3 mm. Filling height of irradiation pits was similar, excluding influence by axial fluence gradients (i.e., variation in flux in the vertical direction of the stacked discs). Assuming equal distribution of grains in the pits, no absolute correction for horizontal fluence gradients need be made when comparing average F values of different samples in one pit. However, given the finite spatial extent of the pits, the fluence gradient adds to the variance of the F values within each pit. Rutte et al. (2015) showed that the three-dimensional variation of neutron fluence in a reactor core is expected to be the result of superposing inverse-square and exponential decay functions. However, over the small extent of the irradiation discs a planar fit is a good first order approximation with residuals of <0.3%, and mostly <0.1%. The computed gradients over individual pits are 0.04% (n = 4; 449a), 0.15% (n = 9; 450PRA), and 0.01% (n = 2; 452A). Thus, within-pit horizontal fluence gradients may explain up to 0.15% of the variance of F values and therefore some excess dispersion in F values (MSWD >1). In irradiation 424, F values of FCs distributed over the disc were used to fit a planar function, representing horizontal variation in neutron fluence (n = 4; 0.21%/cm, residuals 0.024%). We normalized all results of this disc, allowing comparison of F values of individual pits to FCs.

2.4. Analytical procedures

All analyses were conducted at the Berkeley Geochronology Center (BGC) on three mass spectrometers dubbed Nexus, MAP 1, and Noblesse.

2.4.1. Nexus and MAP 1

Irradiation 450PRA consisted of an eleven pit 18.54-mm aluminum disc irradiated for 4 h. The five large pits of the disc were loaded with an even mixture of ACs and Mes4 in order to eliminate uncertainties in the neutron fluence between pits. Six additional small pits contained only ACs in order to provide additional control of neutron fluence across the disc area. Two large pits from this irradiation were analyzed on MAP 1. Three large pits of mixed ACs and Mes4 as well as the six pits containing only ACs from irradiation 450PRA were analyzed on Nexus. Both MAP instruments have Nier-type ion sources and analog electron multiplier

detectors.

Single grains from the large pits of mixed ACs/Mes4 underwent total laser fusion from a CO_2 laser at 8 W of power. ACs samples from small pits were measured by laser fusion analyses of 3-grain aliquots that were used only in the evaluation of fluence gradients and not in any calculations of R values.

For each sample, blank, and air pipette, fifteen cycles at 8–35 integrations per cycle were measured for each Ar isotope using peak hopping by magnetic field switching on a single detector. Evolved gases were cooled to ca. −100 to −130 °C using a cryotrap and exposed to a ca. 450 °C hot getter to remove reactive gases.

For each large pit of ACs/Mes4, a mean blank correction was determined using background isotopic measurements analyzed between each single-grain analysis. Blanks between sample measurements were stationary over time, and mean values and their standard deviations were used to correct the data for unknowns and air pipettes. For Nexus runs, blanks were $3–4 \times 10^{-17}$, $5–15 \times 10^{-19}$, and $7–8 \times 10^{-19}$ mol for ^{40}Ar, ^{39}Ar and ^{36}Ar, respectively. For MAP 1 runs, blanks were $1–2 \times 10^{-16}$, $1–2 \times 10^{-18}$, and $2–3 \times 10^{-19}$ mol for ^{40}Ar, ^{39}Ar and ^{36}Ar, respectively.

Mass discrimination was determined based on automated analyses of air pipettes between every five single grain analyses (plus intercalated blanks) using air pipette data based on a power law correction (Renne et al., 2009) and the atmospheric values of Lee et al. (2006); values of 1.0099–1.0104 and 1.0126 per Dalton were determined for Nexus and MAP 1, respectively.

2.4.2. Noblesse

Samples analyzed on the Noblesse multicollector mass spectrometer were irradiated in three separate batches. Irradiations 449 and 452A contained pits loaded with crystals of more than one sample: 449 had four pits with both ACs and FCs standards, and 452A had four pits loaded with both of these as well as with Mes4. Irradiations 449 and 452A, like 450PRA, allow direct comparison of F values for evaluation of R without necessarily accounting for differences in neutron fluence.

The samples analyzed using the Noblesse multicollector instrument were degassed by incremental heating on a dedicated extraction line. Quasi-uniform heating of each sample (a single grain of sanidine) was achieved via illumination with a CO_2 laser fitted with a beam-shaping lens to generate a flat energy profile of adjustable diameter, typically 2 mm at the target distance. Individual grains of sanidine were heated for ~30 s at progressively increasing power levels (0.9–8 W) until fusion was achieved; typically 3–10 steps were employed for ACs, Mes4, and A1, and 4–13 steps for FCs. Evolved gas was exposed for several minutes to an approximately −130 °C cryotrap to remove H_2O, and to a GP-50 SAES getter to remove reactive gases.

Ar isotopic measurements were performed on a Noblesse 5-collector sector-magnet mass spectrometer, configured with one axial Faraday detector and four off-axis, symmetrically arrayed ETP ion counters. Prior to inlet of sample gas from the extraction line for determination of Ar isotopic composition, a 3% aliquot of the extraction line volume was measured on the mass spectrometer within a short (~7 s) interval. On the basis of this brief measurement, adjustments were made as necessary to the sample abundance by pumping away a calibrated fraction of the gas to evacuated ballast volumes. The goal of this procedure was to restrict the signal level of ^{40}Ar on the ion counters to less than ~500 kcps across all experiments, corresponding to a maximum ^{40}Ar of ~6×10^{-15} mol. Typically, volume splitting was unnecessary, given careful adjustment of the step-heating schedule. Subsequent to this test protocol, the remainder of the sample gas was inlet to the mass spectrometer and five Ar isotopes were measured over a period of ~800 s. The isotopic measurement process involved simultaneous

Table 3
Weighted mean *F* values of individual pits from all irradiations in this study.

Irradiation	Pit #	Lab ID	Sample	Wtd. Mean *F*	±(abs.)	±(%)	Number of grains included (excluded)[a]
450PRA	6	37049	ACs	0.61929	0.00045	0.074	28 (1)
			Mes4	3.5532	0.0011	0.032	30 (2)
	7	37050	ACs	0.61972	0.00043	0.069	22 (2)
			Mes4	3.5653	0.0008	0.022	23 (0)
	8	37051	ACs	0.62072	0.00052	0.084	30 (0)
			Mes4	3.5622	0.0010	0.029	32 (1)
	9	37052	ACs	0.62315	0.00074	0.12	30 (0)
			Mes4	3.5798	0.0016	0.044	26 (3)
	10	37053	ACs	0.62453	0.00073	0.12	25 (0)
			Mes4	3.5882	0.0012	0.033	26 (0)
424	13	26441	ACs	0.25263	0.00029	0.11	14 (1)
	3	26430	Mes4	1.45013	0.00072	0.050	12 (1)
	7	26434	Mes4	1.44807	0.00064	0.044	13 (2)
	11	26438	Mes4	1.45128	0.00063	0.043	14 (0)
	15	26442	Mes4	1.45161	0.00068	0.047	14 (0)
	6	26433	A1	1.47732	0.00082	0.056	15 (0)
	16	26443	A1	1.48139	0.00094	0.063	17 (0)
	1	26428	FCs	6.0471	0.0024	0.039	11 (0)
	5	26432	FCs	6.0443	0.0026	0.043	10 (0)
	9	26436	FCs	6.0433	0.0021	0.035	10 (0)
	13	26440	FCs	6.0515	0.0025	0.041	10 (0)
449	1	27023	ACs	0.8583	0.0010	0.11	7 (1)
		27010	FCs	20.646	0.012	0.058	6 (0)
	4	27026	ACs	0.86083	0.00085	0.10	11 (0)
		27013	FCs	20.6600	0.0092	0.044	7 (0)
	7	27028	ACs	0.86173	0.00091	0.11	10 (0)
		27016	FCs	20.6288	0.0087	0.042	7 (0)
	10	27030	ACs	0.85600	0.00079	0.09	9 (1)
		27019	FCs	20.6289	0.0088	0.043	6 (0)
452A	1	27127	ACs	0.83806	0.00088	0.10	11 (1)
		27126	Mes4	4.8128	0.0022	0.046	10 (0)
		27114	FCs	20.0787	0.0069	0.034	9 (0)
	4	27130	ACs	0.83671	0.00088	0.10	9 (0)
		27129	Mes4	4.8072	0.0023	0.048	10 (0)
		27117	FCs	20.0738	0.0064	0.032	9 (0)

[a] Filtered with a normalized median absolute deviation (nMAD) threshold of 3

measurement of ^{40}Ar, ^{37}Ar, and ^{36}Ar on separate ion counters, alternating with peak hopping to position ^{38}Ar and ^{39}Ar on the same ion counter as ^{40}Ar. All signals were normalized to the ^{40}Ar ion counter. ^{36}Ar signal normalization was achieved through periodic measurement of the ^{40}Ar/^{36}Ar ratio of air argon (Lee et al., 2006) inlet from an air-reservoir pipetting system. Ar abundance from air aliquots experiments was closely matched to the unknowns, yielding 2.3×10^{-15} mol ^{40}Ar. ^{37}Ar and ^{38}Ar signal normalizations were achieved through periodic measurement of ^{40}Ar from a static gas sample on relevant detectors in a systematic round-robin peak-hopping procedure.

Procedural blanks, matching sample gas extractions precisely but without firing the laser, were run every four analyses and typically yielded ~6×10^{-17}, 4×10^{-19}, and 4×10^{-19} mol of ^{40}Ar, ^{39}Ar, and ^{36}Ar, respectively. Blanks preceding air pipette measurements were tailored specifically to mimic an actual air pipette extraction, with the exception that the inner pipette valve leading to the air reservoir was not opened. The Noblesse has sufficiently high resolution to distinguish an almost entirely hydrocarbon free shoulder at mass 36, where the measurement for ^{36}Ar is made. For further details of the analytical procedures refer to Deino et al. (2010).

3. Results

3.1. R values

Results in terms of inverse variance weighted mean *F* values for each sample in each irradiation position are shown in Table 3 and Supplementary Figs. 1—5. For all of the *Noblesse* data, which were

analyzed by incremental heating, the integrated results were used for the most appropriate comparison with total fusion results from Nexus and MAP 1. Step heating data are provided as individual steps in Supplementary Table 1. 13 of 85 step heating results of FCs (Supplementary Fig. 6) are identified as clearly rising after the first step; 5 of these had integrated ages above the mean and 8 of them had integrated ages below the mean. However, using the same nMAD > 3 filter as used for calculating weighted mean *F* values, calculation of integrated ages shows no significant affect to the weighted mean age of FCs for these spectra. While some recent studies (e.g., Phillips and Matchan, 2013; Jicha et al., 2016) have suggested that FCs is a non-ideal standard due to variations in age spectra, our data reveal little evidence to question the suitability of FCs as a standard for high-precision ^{40}Ar/^{39}Ar geochronology based on total gas measurements. Likewise, our step heating results for ACs produce consistent flat age spectra and a well-constrained distribution of total gas ages (MSWD = 1.94) for 71 out of 72 analyses (Supplementary Fig. 7), unlike that indicated by Jicha et al. (2016). Step heating results for Mes4 and A1 can also be found as Supplementary Figs. 8—9. For irradiations 449 (FCs and ACs), 450PRA (ACs and Mes4) and 452A (ACs, Mes4, and FCs), the samples were co-irradiated in the same disc position and the corresponding *R* values for each position are shown in Table 4. For irradiation 424 (ACs, Mes4, A1, and FCs) each sample was irradiated in a separate pit and the *R* values between each of the samples was determined by interpolation. For the determination of *F* values for each position we used an nMAD > 3 (normalized median absolute deviation from the median) criterion to define outliers which were then excluded from further calculations; on this basis 16 of 549 analyses were excluded. *R* values were then computed from the

Table 4

R values from co-irradiated samples in irradiations 450PRA, 452A, and 449, and calculated R values from irradiation 424 as described in the text. Under R_{FCs}^{Mes4} the four pits of Mes4 in irradiation 424 are given as a weighted mean R value (details in text).

Lab ID	R_{Mes4}^{ACs}	±(abs.)	±(%)	Irradiation
37049	0.174292	0.000140	0.080372	450PRA
37050	0.173821	0.000126	0.072562	450PRA
37051	0.174253	0.000154	0.088388	450PRA
37052	0.174074	0.000220	0.126425	450PRA
37053	0.174051	0.000213	0.122101	450PRA
27127/27126	0.174232	0.000319	0.183017	452A
27130/27129	0.174152	0.000430	0.247127	452A
$(R_{FCs}^{ACs})/(R_{FCs}^{Mes4})$	0.174193	0.000289	0.165648	424
Lab ID	R_{FCs}^{Mes4}	**±(abs.)**	**±(%)**	**Irradiation**
27126/27114	0.239551	0.000177	0.073805	452A
27129/27117	0.239339	0.000159	0.066558	452A
Irr. 424	0.239694	0.000089	0.037166	424
Lab ID	R_{FCs}^{ACs}	**±(abs.)**	**±(%)**	**Irradiation**
27127/27114	0.041737	0.000070	0.167476	452A
27130/27117	0.041682	0.000099	0.237995	452A
27023/27010	0.041546	0.000050	0.121312	449
27026/27013	0.041671	0.000045	0.107029	449
27028/27016	0.041773	0.000044	0.104135	449
27030/27019	0.041672	0.000042	0.100786	449
26441	0.041753	0.000067	0.161425	424
Calculated	0.041655	0.000035	0.083354	R_{Mes4}^{ACs}(450PRA) $\times R_{FCs}^{Mes4}$ (Kuiper et al., 2008)
Irradiation 424 individual pit R values vs. FCs				
Lab ID	R_{FCs}^{Unk}	**±(abs)**	**±(%)**	**Sample ID "Unk"**
26430	0.239658	0.000214	0.089085	Mes4
26433	0.244508	0.000251	0.102614	A1
26434	0.239524	0.000145	0.060662	Mes4
26438	0.239932	0.000194	0.080648	Mes4
26441	0.041753	0.000067	0.160948	ACs
26442	0.239779	0.000183	0.076154	Mes4
26443	0.244866	0.000252	0.102954	A1

appropriate F values per Equation (3).

Determinations of R values relating the various samples are presented in matrix form as shown in Table 5. The R matrix provides a summary of intralaboratory weighted mean R values between any two standards. The column header indicates the numerator of the R value and the row header indicates the denominator. These R values may be used to integrate these data with previous and future data sets. Our seven new direct measurements of R_{FCs}^{ACs} (weighted mean $R_{FCs}^{ACs} = 0.041689 \pm 0.000020$) are consistent with values obtained using Mes4 or A1 as intermediaries (weighted means $R_{FCs}^{ACs} = 0.041714 \pm 0.000020$ and 0.041753 ± 0.000080, respectively). We take the weighted mean ($R_{FCs}^{ACs} = 0.041702 \pm 0.000014$, 0.033%) of these three determinations as the best estimate of our intralaboratory value.

3.2. Comparison with previous data

Our direct determination of R_{FCs}^{ACs} can be compared with previous results shown in Table 1 (Fig. 2). Results differ significantly from pre-2006 studies (Turrin et al., 1994; Renne et al., 1998; Nomade et al., 2005), all of which were conducted at BGC. Several factors render our new data superior to those of the previous studies: (1) The spatial density of neutron fluence monitoring is much higher, including many co-irradiations in the same pit; (2) Choice of grain sizes and irradiation durations to optimize ^{39}Ar and ^{40}Ar ion beams and their ratios; (3) Use of 15 cycles of peak-hopping (versus 7–10 cycles in the previous studies) on the single-collector (MAP) instruments provides more accurate constraints on the intercepts of ion beam intensity versus time, particularly for ^{36}Ar; (4) More

integrations per cycle were employed for ^{36}Ar and ^{39}Ar for the MAP data, further enhancing the accuracy of ion beam intercepts. Hence, pre-2006 results are excluded based on our well-informed confidence in the superiority of the new data. The results of Coble et al. (2011), McDougall et al. (2012), and Singer (2014) are relatively imprecise and compatible with a large range of values; hence these are excluded. We attempted to include the data of Jicha et al. (2016), obtained from the same preparation of ACs as ours, by computing total gas results for their incrementally-heated ACs samples. The uncertainties we calculate from their data are larger than reported. The MSWD calculated for R_{FCs}^{ACs} from total gas results of Jicha et al. (2016) (computed from incremental heating data) is 31.4, much larger than the value of 6.41 determined from their single step fusion results. Our own total gas results for R_{FCs}^{ACs}, obtained with an identically configured mass spectrometer are significantly less scattered with an MSWD value of 2.03. We suspect that Jicha et al. (2016) underestimated contributions from background or interference corrections resulting in spuriously high precision and resultant overdispersion of their data. For these reasons, we exclude the results of Jicha et al. (2016) from our interlaboratory compilation despite their reported R_{FCs}^{ACs} being indistinguishable from our own. Our new results can be most appropriately be compared with Rivera et al. (2013) and Phillips and Matchan (2013). We note that the latter study used 2–3 grains of ACs for their step-heating analyses (D. Phillips, written communication, 2014), in contrast to all other data considered here which are based on analysis of single crystals. The weighted mean R_{FCs}^{ACs} of these three sets of experiments is 0.041702 ± 0.000011 (0.026%).

A stepwise determination of R_{FCs}^{ACs} may be calculated using Mes4

Table 5
Matrix of intralaboratory weighted mean *R* values for all iterations of the four samples evaluated.

R_{Row}^{Column}	ACs	Mes4	A1	FCs
ACs	1	5.743859 ± 0.002195 (±0.038%)	5.860311 ± 0.010375 (±0.177%)	23.993239 ± 0.009950 (±0.041%)
Mes4	0.174099 ± 0.000067 (±0.038%)	1	1.020825 ± 0.000833 (±0.082%)	4.173618 ± 0.001240 (±0.030%)
A1	0.170639 ± 0.000302 (±0.177%)	0.979600 ± 0.000800 (±0.082%)	1	4.086868 ± 0.002970 (±0.073%)
FCs	0.041678 ± 0.000017 (±0.041%)	0.239600 ± 0.000071 (±0.030%)	0.244686 ± 0.000178 (±0.073%)	1

as an intermediary. Our eight independent measurements of R_{Mes4}^{ACs} are the first of which we are aware and these form a coherent data set with a weighted mean of 0.174099 ± 0.000067 (0.038%). Our three new measurements of R_{FCs}^{Mes4} compare reasonably well with those of Kuiper et al. (2008), and accordingly we combine our data with the latter to yield an interlaboratory value of 0.239555 ± 0.000066 (0.027%). The corresponding stepwise value of $R_{FCs}^{ACs} = R_{Mes4}^{ACs} \cdot R_{FCs}^{Mes4}$ is 0.041706 ± 0.000020 (0.047%).

A second stepwise determination of R_{FCs}^{ACs} is calculated using A1 as an intermediary. Our data yield a value of 0.041753 ± 0.000080 (0.191%), which may be compared with a value of 0.041753 ± 0.000043 (0.104%) determined from the data of Rivera et al. (2011, 2013). The interlaboratory weighted mean of both results gives $R_{FCs}^{ACs} = 0.041753 \pm 0.000038$ (0.091%).

The three distinct approaches to determining R_{FCs}^{ACs} using interlaboratory data as discussed above are summarized in Table 6. As shown, these result in a weighted mean $R_{FCs}^{ACs} = 0.041707 \pm 0.000011$ (0.026%), which we recommend as an interlaboratory value.

3.3. Age of ACs

In the foregoing we have derived interlaboratory values for the intercalibration of ACs with several other standards. These values are based on analysis in three different laboratories, using five different mass spectrometers (three multi-collector and two single collector) employing a variety of analytical protocols. We turn now to the issue of the age of the ACs standard.

3.3.1. Age based on astrochronology of Mes4

Using our results for R_{Mes4}^{ACs}, the astrochronologic age of $t_{Mes4} = 6.791 \pm 0.005$ Ma (Kuiper et al., 2008), the ^{40}K total decay constant of $5.463 \pm 0.107 \times 10^{-10}$ a^{-1} (Min et al., 2000), Equations (5) and (6) of (Renne et al., 1998) yield

3.3.2. Age based on astrochronology of A1

Our results for R_{A1}^{ACs} combined with the R_{A1}^{ACs} value in Table 1 of Rivera et al. (2013) (0.170462 ± 0.000313) yield a weighted mean value of 0.17055 ± 0.00022 (0.127%). Substituting this value and the astrochronologic age of 6.943 ± 0.0025 Ma for the A1 tephra into the above Equation (5) yields an independent astronomical age ($t_{ACs} = 1.1860 \pm 0.0016$ Ma) that is indistinguishable from that based on Mes4 (although less precise because *R* was less well determined).
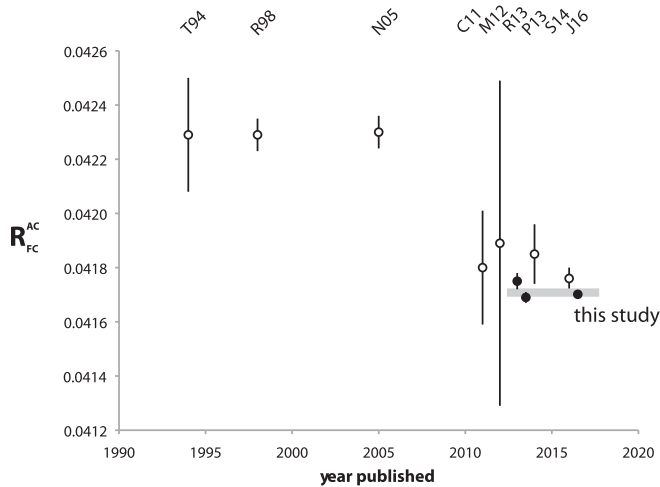
3.3.3. Ages based on intercalibration with FCs

Using our preferred interlaboratory value of $R_{FCs}^{ACs} = 0.041707 \pm 0.000011$ (Table 6), we can calculate an astronomical age for ACs based on the astronomical calibration of FCs from Messâdit (Kuiper et al., 2008). This is not strictly independent of the foregoing results based on Mes4, because data from Mes4 were included in that calibration. Using the astrochronological age of 28.201 ± 0.022 Ma for FCs (Kuiper et al., 2008), using the uncertainty which neglects contribution from the decay constant, and applying Equation (5) with appropriate substitutions, yields $t_{ACs} = 1.1849 \pm 0.0009$ Ma, in excellent agreement with the other two astronomically-calibrated ages. Although these three ages are not strictly independent, we take the weighted mean $t_{ACs} = 1.1848 \pm 0.0006$ Ma (0.052%) as the best representation of all available astronomical constraints on the age of ACs.

A fundamentally different approach uses the so-called optimization calibration of (Renne et al., 2011), which is based on an optimal fit to ^{40}K disintegration data, K and Ar isotopic data for the FCs standard, and pairs of ^{40}Ar/^{39}Ar and ^{238}U-^{206}Pb data representing a partial normalization to the ^{238}U decay constant. Using our preferred interlaboratory value of R_{FCs}^{ACs} as above applied to the calibration of Renne et al. (2011) yields $t_{ACs} = 1.1891 \pm 0.0008$ Ma, which is distinct at 95% confidence from the Mes4 and FCs based astronomically calibrated ages outlined above, but not from the less precisely determined age based on A1. However, all of these ages (Table 7) are younger than the younger mode of ^{238}U-^{206}Pb zircon ages (1.1978 ± 0.0023 Ma) inferred by Rivera et al. (2013) for the Alder Creek rhyolite based on the likelihood of pre-eruptive residence time of zircons in silicic magmas (Simon et al., 2008).

3.4. Recoil?

The data from irradiation 450PRA, wherein two different size fractions of Mes4 were co-irradiated with a single size fraction of ACs, can be used to evaluate the possibility of age bias due to differential ^{39}Ar recoil effects (Hall, 2014). The ratio of ^{39}Ar ion beams for ACs relative to Mes4 for the two positions with larger Mes4 grains is ~0.68, whereas for the three positions with smaller Mes4 grains the average ratio is ~1.60. *R* shows no correlation with the relative ^{39}Ar ion beams, from which we conclude that any bias due to differential ^{39}Ar recoil effects is negligible owing to the close match in grain sizes. Hence the fractional ^{39}Ar recoil loss from each sample is comparable, and the effect on the computed *R* values is negligible as the fraction retained is the same in the *F* values comprising the numerator and the denominator.

$$t_{ACs} = \frac{1}{5.463 \times 10^{-10} a^{-1}} \ln\left[\left(e^{(5.463 \times 10^{-10} a^{-1})(6.791 \times 10^6 a)} - 1 \right)(0.174099) + 1 \right] = 1.1841 \pm 0.00098 \text{ Ma} \qquad (5)$$

Fig. 2. Compilation of R_{FCs}^{ACs} values from previous publications and this work (T94: Turrin et al. (1994); R98: Renne et al. (1998); N05: Nomade et al. (2005); C11: Coble et al. (2011); M12: McDougall et al. (2012); R13: Rivera et al. (2013); P13: Phillips and Matchan (2013); S14: Singer (2014); J16: Jicha et al. (2016). Solid circles identify R_{FCs}^{ACs} that were incorporated into the weighted mean interlaboratory R_{FCs}^{ACs} represented by the shaded gray bar (see text for justification).

Table 6
Interlaboratory values of R_{FCs}^{ACs} obtained by different methods.

Method	R_{FCs}^{ACs}	$\pm\sigma$	$\pm\sigma$ (%)
Direct	0.041702	0.000011	0.03%
Via Mes4	0.041706	0.000020	0.05%
Via A1	0.041753	0.000038	0.09%
Weighted Mean	**0.041707**	**0.000011**	**0.03%**

3.5. Application to the Matuyama-Brunhes boundary (MBB)

As the most recent non-excursional geomagnetic polarity reversal, the Matuyama/Brunhes boundary (MBB) is arguably the single most referenced magnetostratigraphic marker in Quaternary chronostratigraphic studies. Estimates of the age of the MBB span >20 ka (Singer, 2014). The most precise datum available for the age of the MBB is from the Sulmona paleolake of central Italy (Sagnotti et al., 2014), where the MBB is tightly bracketed by $^{40}Ar/^{39}Ar$ dates on sanidine from intercalated tephras, and was dated to 786.1 ± 0.8 ka based on the ACs age calibration of Nomade et al. (2005) and the decay constants of Steiger and Jäger (1977). This age corresponds to a value of $R_{ACs}^{MBB} = 0.65830 \pm 0.00067$, which combined with our values of R_{Mes4}^{ACs} and R_{A1}^{ACs} yields indistinguishable ages of 779.6 ± 1.0 ka and 780.8 ± 1.3 ka for astronomical ages based on Mes4 and A1, respectively. These two independent calibrations yield a weighted mean age for the MBB of 780.1 ± 0.8 ka. The optimization

Table 7
Summary of ages for ACs. Astronomical result shows the weighted mean of three ages via FCs, Mes4, and A1 calibrations above. Optimization result shows the age of ACs using the weighted mean interlaboratory R_{FCs}^{ACs} in the optimization calibration (Renne et al., 2011).

Method	Age of ACs (Ma)	± σ (Ma)	± σ (%)
Via FCs[a]	1.1849	0.0009	0.08%
Via Mes4	1.1841	0.0010	0.08%
Via A1	1.1860	0.0016	0.13%
Astronomical	**1.1848**	**0.0006**	**0.05%**
Optimization	**1.1891**	**0.0008**	**0.07%**

[a] Based on all Messàdit section tuning data of Kuiper et al., 2008

calibration (Renne et al., 2011) of ACs applied to the MBB yields an age of 782.8 ± 1.0 ka, indistinguishable from either of the independent astronomical ages or their weighted mean mainly due to the relatively large uncertainty in R_{ACs}^{MBB}. All of these results are significantly older than the age of 773.1 ± 0.4 ka for the MBB inferred by Channell et al. (2010) based on correlation of marine oxygen isotope records to an orbitally tuned ice-volume model. While this discrepancy may have important implications for paleoceanography and/or geomagnetic field behavior, such issues are beyond the scope of this paper.

4. Conclusions

Our new $^{40}Ar/^{39}Ar$ measurements of the ACs standard relative to the widely-used FCs standard, directly as well as through an intermediate step using two astronomically dated sanidines (Mes4 and A1), enable determination of R_{FCs}^{ACs} that is consistent with other recent measurements of this parameter, yielding an interlaboratory value with relative uncertainty of 0.026%. The resulting improvement in interlaboratory consistency is reassuring, but does not completely resolve the issue of absolute calibration as the weighted mean astronomical age (1.1848 ± 0.0006 Ma) differs significantly (by 0.36%) from the optimization calibrated age (1.1891 ± 0.0008 Ma).

Application of the interlaboratory data to the most precise $^{40}Ar/^{39}Ar$ data for the age of the Matuyama-Brunhes boundary (Sagnotti et al., 2014) yields ages for the boundary of 780.1 ± 0.8 ka (weighted mean astronomical age) and 782.8 ± 1.0 ka (optimization age) which are indistinguishable at the 95% confidence level. Both of these ages are distinctly older than that ascribed to the MBB by Channell et al. (2010).

Our results compared with the ^{238}U-^{206}Pb zircon data (Rivera et al., 2013) indicate that zircons from the Alder Creek rhyolite record 13 ± 2 (based on the astronomical age of ACs) or 9 ± 2 ka (based on the optimization age of ACs) of pre-eruptive magma residence time. This conclusion agrees with that of Rivera et al. (2013), and it is noteworthy because it indicates that even the youngest mode of zircon U-Pb ages pre-dates eruption by a resolvable interval (assuming that the $^{40}Ar/^{39}Ar$ system accurately records the time of eruption). In this case the bias is small compared with some other examples (Simon et al., 2008; Wotzlaw et al., 2014), but it raises the question of what distinct petrologic event, if any, is recorded by zircon U-Pb ages in cases wherein a well-defined and geochemically distinct youngest age mode is present. If such modes represent the integrated history of zircon crystallization (Ickert et al., 2015), then they may cluster well but still be biased by tens or hundreds of ka relative to the eruption age.

Appendix A. Supplementary data

Supplementary data related to this article can be found at http://dx.doi.org/10.1016/j.quageo.2016.09.004.

References

Channell, J.E.T., Hodell, D.A., Singer, B.S., Xuan, C., 2010. Reconciling astrochronological and ^{40}Ar/^{39}Ar ages for the Matuyama-Brunhes boundary and late Matuyama. Chron. Geochem. Geophys. Geosyst. 11.

Channell, J.E.T., Mazaud, A., Sullivan, P., Turner, S., Raymo, M.E., 2002. Geomagnetic excursions and paleointensities in the MatuRes. Solidyama chron at ocean drilling program sites 983 and 984 (Iceland basin). J. Geophys. Res. Solid Earth 107.

Coble, M.A., Grove, M., Calvert, A.T., 2011. Calibration of Nu-Instruments Noblesse multicollector mass spectrometers for argon isotopic measurements using a newly developed reference gas. Chem. Geol. 290, 75–87.

Deino, A.L., Scott, G.R., Saylor, B., Alene, M., Angelini, J.D., Haile-Selassie, Y., 2010. ^{40}Ar/^{39}Ar dating, paleomagnetism, and tephrochemistry of Pliocene strata of the hominid-bearing Woranso-Mille area, west-central Afar Rift, Ethiopia. J. Hum. Evol. 58, 111–126.

Hall, C.M., 2014. Direct measurement of recoil effects on ^{40}Ar/^{39}Ar standards. In: Advances in ^{40}Ar/^{39}Ar Dating: from Archaeology to Planetary Sciences, vol. 378, pp. 53–62.

Horng, C.S., Lee, M.Y., Palike, H., Wei, K.Y., Liang, W.T., 2002. Astronomically calibrated ages for geomagnetic reversals within the Matuyama chron. Earth Planets Space 54, 679–690.

Ickert, R.B., Mundil, R., Magee Jr., C.W., Mulcahy, S.R., 2015. The U-Th-Pb systematics of zircon from the Bishop Tuff: a case study in challenges to high-precision Pb/U geochronology at the millenial scale. Geochim. Cosmochim. Acta 168, 88–110.

Jicha, B.R., Singer, B.S., Sobol, P., 2016. Re-evaluation of the ages of ^{40}Ar/^{39}Ar sanidine standards and supereruptions in the western US using a Noblesse multicollector mass spectrometer. Chem. Geol. 431, 54–66.

Kuiper, K.F., Deino, A., Hilgen, F.J., Krijgsman, W., Renne, P.R., Wijbrans, J.R., 2008. Synchronizing rock clocks of Earth history. Science 320, 500–504.

Kuiper, K.F., Hilgen, F.J., Steenbrink, J., Wijbrans, J.R., 2004. ^{40}Ar/^{39}Ar ages of tephras intercalated in astronomically tuned Neogene sedimentary sequences in the eastern Mediterranean. Earth Planet. Sci. Lett. 222, 583–597.

Lee, J.Y., Marti, K., Severinghaus, J.P., Kawamura, K., Yoo, H.S., Lee, J.B., Kim, J.S., 2006. A redetermination of the isotopic abundances of atmospheric Ar. Geochim. Cosmochim. Acta 70, 4507–4512.

McDougall, I., Brown, F.H., Vasconcelos, P.M., Cohen, B.E., Thiede, D.S., Buchanan, M.J., 2012. New single crystal ^{40}Ar/^{39}Ar ages improve time scale for deposition of the Omo Group, Omo-Turkana Basin, East Africa. J. Geol. Soc. 169, 213–226.

Min, K.W., Mundil, R., Renne, P.R., Ludwig, K.R., 2000. A test for systematic errors in ^{40}Ar/^{39}Ar geochronology through comparison with U/Pb analysis of a 1.1-Ga rhyolite. Geochim. Cosmochim. Acta 64, 73–98.

Nomade, S., Renne, P.R., Vogel, N., Deino, A.L., Sharp, W.D., Becker, T.A., Jaouni, A.R., Mundil, R., 2005. Alder Creek sanidine (ACs-2): a Quaternary ^{40}Ar/^{39}Ar dating standard tied to the Cobb Mountain geomagnetic event. Chem. Geol. 218, 315–338.

Phillips, D., Matchan, E.L., 2013. Ultra-high precision ^{40}Ar/^{39}Ar ages for fish Canyon tuff and Alder Creek rhyolite sanidine: new dating standards required? Geochim. Cosmochim. Acta 121, 229–239.

Renne, P.R., Balco, G., Ludwig, K.R., Mundil, R., Min, K., 2011. Response to the comment by W.H. Schwarz et al. on "Joint determination of ^{40}K decay constants and ^{40}Ar*/^{40}K for the Fish Canyon sanidine standard, and improved accuracy for ^{40}Ar/^{39}Ar geochronology" by PR Renne, et al. (2010). Geochim. Cosmochim. Acta 75, 5097–5100.

Renne, P.R., Cassata, W.S., Morgan, L.E., 2009. The isotopic composition of atmospheric argon and ^{40}Ar/^{39}Ar geochronology: time for a change? Quat. Geochronol. 4, 288–298.

Renne, P.R., Swisher, C.C., Deino, A.L., Karner, D.B., Owens, T.L., DePaolo, D.J., 1998. Intercalibration of standards, absolute ages and uncertainties in ^{40}Ar/^{39}Ar dating. Chem. Geol. 145, 117–152.

Renne, P.R., Sprain, C.J., Richards, M.A., Self, S., Vanderkluysen, L., Pande, K., 2015. State shift in Deccan volcanism at the Cretaceous-Paleogene boundary, possibly induced by impact. Science 350, 76–78.

Rivera, T.A., Storey, M., Schmitz, M.D., Crowley, J.L., 2013. Age intercalibration of ^{40}Ar/^{39}Ar sanidine and chemically distinct U/Pb zircon populations from the Alder Creek Rhyolite Quaternary geochronology standard. Chem. Geol. 345, 87–98.

Rivera, T.A., Storey, M., Zeeden, C., Hilgen, F.J., Kuiper, K., 2011. A refined astronomically calibrated ^{40}Ar/^{39}Ar age for Fish Canyon sanidine. Earth Planet. Sci. Lett. 311, 420–426.

Rutte, D., Pfander, J.A., Koleska, M., Jonckheere, R., Unterricker, S., 2015. Radial fast-neutron fluence gradients during rotating ^{40}Ar/^{39}Ar sample irradiation recorded with metallic fluence monitors and geological age standards. Geochem. Geophys. Geosyst. 16, 336–345.

Sagnotti, L., Scardia, G., Giaccio, B., Liddicoat, J.C., Nomade, S., Renne, P.R., Sprain, C.J., 2014. Extremely rapid directional change during Matuyama-Brunhes geomagnetic polarity reversal. Geophys. J. Int. 199, 1110–1124.

Shackleton, N.J., Berger, A., Peltier, W.R., 1990. An alternative astronomical calibration of the lower Pleistocene timescale based on ODP site 677. Trans. R. Soc. Edinburgh-Earth Sci. 81, 251–261.

Simon, J.I., Renne, P.R., Mundil, R., 2008. Implications of pre-eruptive magmatic histories of zircons for U-Pb geochronology of silicic extrusions. Earth Planet. Sci. Lett. 266, 182–194.

Singer, B.S., 2014. A Quaternary geomagnetic instability time scale. Quat. Geochronol. 21, 29–52.

Steiger, R.H., Jäger, E., 1977. Subcommission on geochronology: convention on use of decay constants in geochronology and cosmochronology. Earth Planet. Sci. Lett. 36, 359–362.

Turrin, B.D., Donnellynolan, J.M., Hearn, B.C., 1994. ^{40}Ar/^{39}Ar ages from the rhyolite of Alder Creek, California: age of the Cobb mountain normal-polarity subchron revisited. Geology 22, 251–254.

Wotzlaw, J.-F., Husing, S.K., Hilgen, F.J., Schaltegger, U., 2014. High-precision zircon U-Pb geochronology of astronomically dated volcanic ash beds from the Mediterranean Miocene. Earth Planet. Sci. Lett. 407, 19–34.